BIOCHEMISTRY

 Volume 43, Number 30 August 3, 2004

Accelerated Publications

Three-Dimensional Structure of an Independently Folded Extracellular Domain of Human Amyloid-β Precursor Protein[†,‡]

Irina Dulubova,*[,§] Angela Ho,[||] Iryna Huryeva,[§] Thomas C. Südhof,[||] and Josep Rizo[§]

Departments of Biochemistry and Pharmacology, Center for Basic Neuroscience, Department of Molecular Genetics, and Howard Hughes Medical Institute, University of Texas Southwestern Medical Center, 5323 Harry Hines Boulevard, Dallas, Texas 75390

Received May 11, 2004; Revised Manuscript Received June 22, 2004

ABSTRACT: Cleavage of amyloid-β precursor protein (APP) by site-specific proteases generates amyloid-β peptides (Aβs), which are thought to induce Alzheimer's disease. We have identified an independently folded extracellular domain of human APP localized proximal to the Aβ sequence, and determined the three-dimensional structure of this domain by NMR spectroscopy. The domain is composed of four α-helices, three of which form a tight antiparallel bundle, and constitutes the C-terminal half of the central extracellular region of APP that has been implicated in the regulation of APP cleavage. Sequence comparisons demonstrate that the domain is highly conserved among all members of the APP family, including invertebrate homologues, suggesting an important role for this region in the biological function of APP. The identification of this domain and the availability of its atomic structure will facilitate analysis of APP function and of the role of the extracellular region in the regulation of APP cleavage.

Amyloid-β precursor protein (APP)[1] is a type 1 membrane glycoprotein composed of a large extracellular sequence, a single transmembrane region, and a short intracellular fragment (Figure 1A). It belongs to a group of ubiquitously expressed cell surface proteins whose heterogeneity arises from both alternative splicing and posttranslational modifications. The alternative splicing results in three major APP isoforms: APP_{695}, APP_{751}, and APP_{770}. In addition to APP, two closely related homologues, APLP1 and APLP2, are expressed in vertebrates (reviewed in refs *1* and *2*). APP and APLPs are physiologically processed by site-specific proteases called α-, β-, and γ-secretases (*1*, *2*). APP cleavage by β- and γ-secretases produces 40−42-residue amyloid-β peptides (Aβs). Aβs form neurotoxic fibrils that are the principal components of the cerebral amyloid plaques characteristic of Alzheimer's disease (AD). The processing of APP has been intensely studied because of its implication in AD, but the precise regulation of cleavage is not well understood. Furthermore, gene knockout experiments revealed that APP and APLPs are essential and partially redundant (*3*, *4*), but their normal physiological functions are unknown.

[†] This work was supported in part by the Alzheimer's Disease Center, University of Texas Southwestern Medical Center at Dallas, Grant P30-AGO12300-10 to I.D., and by NIH Grant R01-MH69585-01 to T.C.S.

[‡] Structures have been deposited in the RCSB Protein Data Bank (entry 1TKN). Assigned chemical shifts are available at BMRB (entry 6236).

* To whom correspondence should be addressed. Phone: (214) 648-8924. Fax: (214) 648-8673. E-mail: Irina.Dulubova@UTSouthwestern.edu.

[§] Departments of Biochemistry and Pharmacology.

[||] Center for Basic Neuroscience, Department of Molecular Genetics, and Howard Hughes Medical Institute.

[1] Abbreviations: APP, amyloid-β precursor protein; Aβ, amyloid-β peptide; AD, Alzheimer's disease; APLP1 and -2, amyloid precursor-like protein-1 and -2, respectively; CAPPD, central APP domain; NMR, nuclear magnetic resonance; HSQC, heteronuclear single-quantum coherence; GdnHCl, guanidinium chloride.

10.1021/bi049041o CCC: $27.50
Published on Web 07/09/2004

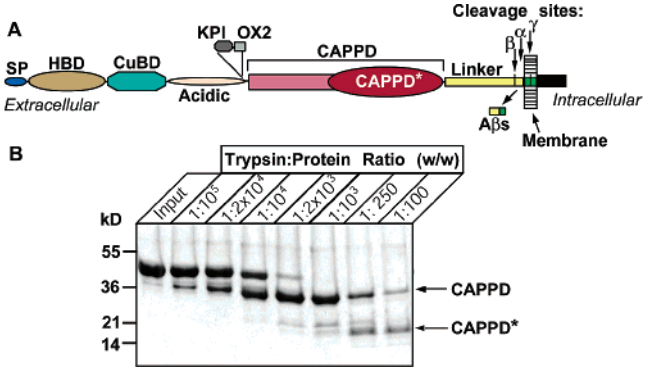

FIGURE 1: Domain structure of the extracellular sequence of human APP and identification of CAPPD*. (A) Summary of known structural information of human APP. SP is the signal peptide, HBD the heparin-binding domain (residues 28−123), CuBD the Cu^{2+}-binding domain (residues 124−189), KPI the Kunitz-type protease inhibitor domain (residues 287−344), OX2 the OX2 homology sequence (residues 345−363), and CAPPD the central APP domain (residues 365−570). (B) Limited proteolysis with trypsin. The samples of human APP recombinant fragment (residues 365−658) incubated for 30 min at room temperature with different amounts of trypsin were analyzed by SDS−PAGE followed by Coomassie blue staining. The enzyme:protein ratio is indicated above each lane. The molecular mass standards are shown at the left.

The extracellular sequences of APP and APLPs consist of a string of characteristic domains (Figure 1A). At the N-terminus, a signal peptide precedes highly conserved N-terminal heparin- and copper-binding domains whose three-dimensional structures have been determined (*5*, *6*). These domains are followed by a highly acidic sequence and two alternatively spliced regions [a Kunitz-type protease inhibitor domain (*7*) and an OX-2 homology sequence]. Both the Kunitz-type protease inhibitor domain and OX-2 sequence are absent from the major neuronal isoform, APP_{695}. The subsequent ~200 amino acids of APP represent its largest conserved region (Figure 2 and Supporting Information Figure 1). This extracellular sequence, termed CAPPD (*8*) (for central APP domain, residues 365−570; the numbering throughout the paper corresponds to the longest splice variant, APP_{770}), is localized close to the β-secretase cleavage site of APP, suggesting that the CAPPD may be involved in the regulation of the cleavage. Indeed, a recent study showed that F-spondin, a secreted neuronal glycoprotein, binds to the CAPPD and modulates APP cleavage (*8*). However, no structural information about the CAPPD is available. In the study presented here, we have identified an independently folded domain within CAPPD, which we call CAPPD*, and determined its three-dimensional structure by multidimensional heteronuclear NMR spectroscopy.

EXPERIMENTAL PROCEDURES

Protein Expression and Purification. DNA constructs for expression of the different fragments of human APP were generated by PCR with custom-designed primers, subcloned into pGEX-KG (*9*) or pGEX-KT (*10*) vectors, and expressed in bacteria (*Escherichia coli* BL21) as GTS fusion proteins. To generate uniformly ^{15}N-labeled or ^{15}N- and ^{13}C-labeled samples for NMR studies, bacteria were grown in minimal medium supplemented with $^{15}NH_4Cl$ or with $^{15}NH_4Cl$ and [$^{13}C_6$]glucose (CIL Inc.) as the sole nitrogen and carbon sources, respectively. Soluble fusion proteins were affinity-purified on glutathione−Sepharose beads (Pharmacia), cleaved from the GST moiety with thrombin, and further purified by ion exchange or size exclusion chromatography. The recombinant protein did not contain any detectable contaminants as judged by SDS−PAGE, the size exclusion chromatography profile, and UV and $^1H-^{15}N$ HSQC spectra.

Limited Proteolysis. The GST−APP recombinant fragment [residues 365−658 of human APP_{770} produced in the pGEX-KG bacterial expression vector (*9*) in ^{15}N-labeled medium] was attached to glutathione−Sepharose beads, cleaved with thrombin, and purified by ion exchange chromatography. Thrombin cleavage generates the recombinant protein bearing an additional N-terminal vector-derived sequence (GSPGISGGGGGILEV) attached to the N-terminus of the APP fragment. Aliquots of the purified recombinant protein were incubated for 30 min at room temperature with different amounts of L-1-tosylamide-2-phenylethylchloromethyl ketone (TPCK)-treated trypsin (Sigma) at the protein:enzyme ratios given in Figure 1B. Proteolytic fragments were separated by SDS−PAGE and identified by N-terminal sequencing and mass spectrometry. The observed molecular mass was 27 573 Da for the intermediate trypsin-resistant fragment and 15 000 Da for the smaller fragment [the calculated molecular mass for the ^{15}N-labeled APP(365−585) with the N-terminal extension is 27 578 Da and for the ^{15}N-labeled APP(461−585) is 15 004 Da].

NMR Spectroscopy. All NMR data were acquired on an INOVA500 spectrometer at 27 °C. Initial $^1H-^{15}N$ HSQC spectra of the APP(460−576) and APP(460−585) fragments were acquired at protein concentrations of 50−60 μM in buffer containing 25 mM sodium phosphate and 150 mM NaCl. Structure elucidation was performed using 0.85 mM uniformly ^{15}N-labeled or ^{15}N- and ^{13}C-labeled samples of the APP(460−576) fragment in buffer containing 50 mM sodium phosphate, 250 mM NaCl, and 300 mM guanidinium chloride (GdnHCl) with 5% ^2H_2O at pH 6.4. Resonance assignments, NOEs, and amide protection data for structural determination were obtained from a series of two-dimensional (2D) and three-dimensional (3D) experiments as described previously (*11*). These experiments included 3D $^1H-^{15}N$ TOCSY-HSQC and NOESY-HSQC, HNCO, HNCACB, CBCA(CO)NH, H(C)(CO)NH-TOCSY (21 ms mixing time), (H)C(CO)NH-TOCSY (21 ms mixing time), and HCCH-TOCSY (14 ms mixing time) spectra for resonance assignments (*12*−*15*), and 2D NOESY, 3D $^1H-^{15}N$ NOESY-HSQC, and 3D $^1H-^{13}C$ NOESY-HSQC spectra (all with a mixing time of 100 ms) for measuring NOEs for structure determination. Protection of amide protons from the solvent was assessed from the intensities of exchange cross-peaks with the water resonance in 3D $^1H-^{15}N$ NOESY-HSQC and TOCSY-HSQC experiments. Stereospecific assignments of valine and leucine methyl groups were obtained from a $^1H-^{13}C$ HSQC spectrum acquired on a 0.8 mM sample of 10% ^{13}C-labeled APP(460−576). All data were processed with NMRPipe (*16*) and analyzed with NMRView (*17*).

Structure Calculations. NOE cross-peak intensities were classified as strong, medium, weak, and very weak and assigned to restraints of 1.8−2.8, 1.8−3.5, 1.8−5.0, and 1.8−6.0 Å, respectively, with appropriate pseudoatom corrections. Backbone torsion angles were derived from chemical shift analysis using TALOS (*18*) and employing the

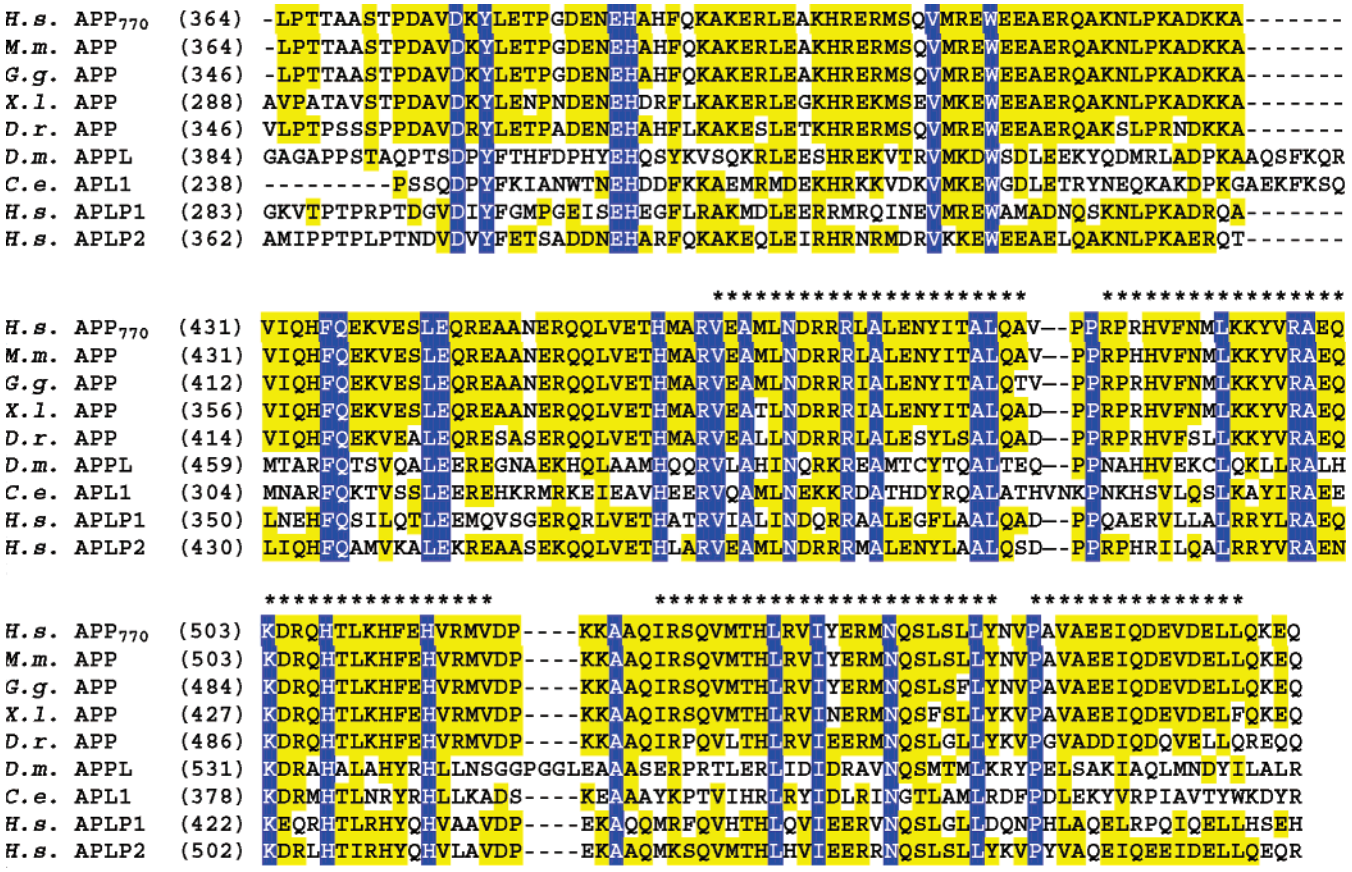

FIGURE 2: Sequence alignment of CAPPD (for an alignment of the full-length sequences of APP/APLP family members, see the Supporting Information). The sequences labeled with asterisks correspond to the four α-helices of the CAPPD*. Identical amino acid residues are shown in white on a blue background, and highly homologous residues (E/D, K/R, N/Q, I/L/V, F/W/Y, and S/T) are highlighted in yellow. Abbreviations: *H.s.* APP_{770}, human (*Homo sapiens*) APP_{770} (GenBank entry NM_000484); *M.m.* APP, mouse (*Mus musculus*) APP (GenBank entry AY267348); *G.g.* APP, chicken (*Gallus gallus*) APP (GenBank entry AF289219); *X.l.* APP, frog (*Xenopus leavis*) APP (GenBank entry AJ298151); *D.r.* APP, zebrafish (*Danio rerio*) APP (GenBank entry AF389401); *D.m.* APPL, fruit fly (*Drosophila melanogaster*) APP (GenBank entry J04516); *C.el.* APL1, *Caenorhabditis elegans* APP (GenBank entry U00240); *H.s.* APLP1, human (*H. sapiens*) APLP1 (GenBank entry NM_005166); *H.s.* APLP2, human (*H. sapiens*) APLP2 (GenBank entry S60099).

standard database provided by the program. Restraints were set at 1.5 times the standard deviation yielded by TALOS (22.5° minimum). Hydrogen bond restraints were 1.7−2.5 and 2.7−3.5 Å for H−O and N−O distances, respectively. Structures were calculated by simulated annealing using torsion angle dynamics with CNS (*19*). The force constants used were 75 kcal mol^{-1} $Å^{-2}$ and 400 kcal mol^{-1} rad^{-2} for distance and torsion angle restraints, respectively. A total of 1000 structures were calculated with the final set of restraints, and the 20 structures with the lowest overall energies were selected.

RESULTS

To structurally characterize the CAPPD, we performed limited proteolysis experiments with a recombinant fragment composed of residues 365−658 of human APP. This fragment, which contains the predicted CAPPD and ∼90 additional residues at the C-terminal end, was chosen because sequence alignments showed that these additional residues are evolutionarily conserved in APP, but not in APLPs (Supporting Information Figure 1). We observed an intermediate trypsin-resistant fragment with a molecular mass of ∼30 kDa that was further proteolyzed to a smaller fragment of ∼15 kDa (Figure 1B). Using mass spectroscopy and N-terminal sequencing, we found that the intermediate fragment corresponds to residues 365−585, matching the CAPPD boundaries predicted by sequence alignments. The smaller fragment arises from trypsin cleavage at two arginine residues, R_{460} and R_{585}, and spans the C-terminal half of the CAPPD. Its resistance to proteolysis suggests that this fragment contains a minimal structural unit within the CAPPD that we termed CAPPD*.

To further characterize CAPPD* and better define its boundaries, we used NMR spectroscopy. Two recombinant ^{15}N-labeled fragments encompassing CAPPD* (residues 460−585 and 460−576) were analyzed. Both recombinant proteins were monomeric under physiological conditions and at protein concentrations of <60 μM, as revealed by their one-dimensional NMR signal line widths and size exclusion chromatography profiles (data not shown). In addition, the excellent dispersion of their $^1H-^{15}N$ heteronuclear single-quantum correlation (HSQC) spectra (Supporting Information Figure 2) confirmed that the fragments contain an independently folded domain. Since the $^1H-^{15}N$ HSQC spectra of both fragments were practically identical and the additional cross-peaks observed for the longer fragment exhibited narrow line widths and poor ^1H chemical shift dispersion characteristic of unstructured polypeptides, we focused on the shorter fragment (residues 460−576) for structure determination. The fragment exhibited a strong tendency to

Table 1: Structural Statistics and Atomic rms Deviations for the 20 Simulated Annealing Structures of CAPPD* with the Lowest Overall Energies[a]

Average rms Deviations from Experimental Restraints (1613 total)	
NOE distance restraints (Å)	
all (1266)	0.008 ± 0.0004
intraresidue (337)	0.007 ± 0.0011
sequential ($\|i - j\| = 1$) (356)	0.009 ± 0.0008
short-range ($\|i - j\| = 2-4$) (434)	0.009 ± 0.0005
long-range ($\|i - j\| > 4$) (139)	0.008 ± 0.0014
hydrogen bonds (Å) (162)	0.008 ± 0.0008
dihedral angles (deg) (185)	0.039 ± 0.017
Average rms Deviations from Idealized Covalent Geometry	
bonds (Å)	0.0015 ± 0.00003
angles (deg)	0.35 ± 0.004
impropers (deg)	0.20 ± 0.009
Ramachandran Plot Statistics (%)[b]	
residues in most favored regions	95.1
residues in additionally allowed regions	3.9
residues in generously allowed regions	1.00
residues in nonallowed regions	0.00
Average rms Deviations of Atomic Coordinates (Å)	
backbone residues 460−569	0.95 ± 0.28
heavy atom residues 460−569	1.67 ± 0.34
backbone secondary structure[c]	0.40 ± 0.14
heavy atom secondary structure[c]	1.24 ± 0.3

[a] None of the structures have distance violations of >0.1 Å or dihedral angle violations of >0.5°. [b] Determined by PROCHECK (*24*). [c] Four α-helices (residues 461−482, 487−518, 526−549, and 552−566).

reversibly aggregate at concentrations of >100 μM under a wide range of conditions that were tested, but became highly soluble in monomeric form at the concentrations required for structure elucidation (close to 1 mM) in the presence of 250 mM NaCl and 300 mM GdnHCl. Comparison of the $^{1}H-^{15}N$ HSQC spectrum of the highly concentrated fragment (0.85 mM) obtained under these conditions with the spectrum recorded at physiological salt concentrations and 60 μM protein revealed only minor perturbations (Supporting Information Figure 2), demonstrating unambiguously that the structure of CAPPD* is not affected by the addition of GdnHCl.

To determine the three-dimensional structure of CAPPD* by NMR, we used a set of standard 2D and 3D double- and triple-resonance experiments as outlined in Experimental Procedures. All backbone ^{1}H, ^{15}N, and ^{13}C resonances of the fragment and all side chain ^{1}H, ^{15}N, and ^{13}C resonances (excluding quaternary carbons and exchangeable protons) were assigned. Analysis of the observed patterns of nuclear Overhauser effects (NOEs) and the deviations of the backbone chemical shifts from random coil values showed that residues 460−569 are structured, which thus defines the boundaries of CAPPD*. Restraints derived from NOEs, chemical shifts, and amide accessibility data were then used to determine the structure of CAPPD* in solution.

A total of 1613 experimental restraints were used to generate a final set of 20 conformers of the domain. The structural statistics are summarized in Table 1, and backbone superpositions of the structures are shown in Figure 3. Ribbon diagrams and space filling models of the lowest-energy structure in two orientations are shown in Figure 4. The quality of the structures is reflected by small deviations from the experimental restraints and from idealized covalent geometry, as well as by the high percentage

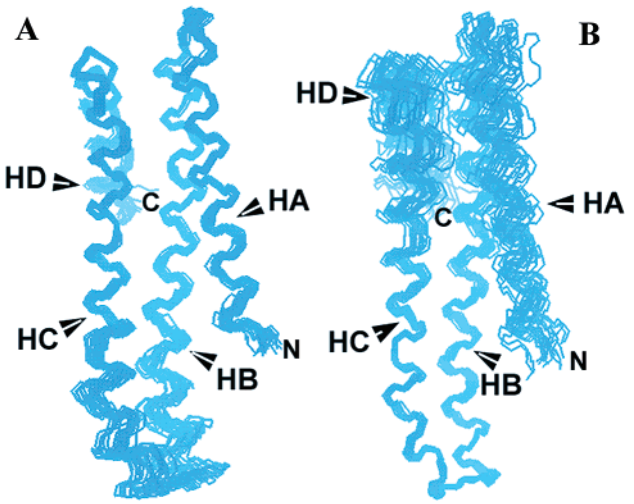

FIGURE 3: Backbone superpositions of the 20 structures of human CAPPD* with the lowest overall energies. Since helix HA of the three-helix bundle is significantly shorter than the other two helices, the relative orientation of the bottom of helices HB and HC with respect to the rest of the domain is poorly defined. Thus, two different backbone superpositions were generated. In panel A, the top part of the domain (residues 463−504 and 537−566) was superimposed, yielding a backbone rms deviation of 0.57 ± 0.18 Å. In panel B, residues constituting the bottom part of the domain (504−537) was superimposed, resulting in a backbone rms deviation of 0.47 ± 0.15 Å.

of residues in the most favored regions of the Ramachandran map (Table 1).

The structure of CAPPD* reveals that the domain is composed of four α-helices connected by short loops and/or turns (Figure 4A,B), in agreement with the secondary structure predicted from the NOE patterns and the backbone chemical shifts. The three N-terminal helices (HA, HB, and HC) form a tight elongated up-and-down bundle, while the fourth helix (HD) "crosses" the top of the bundle. Helix HA is significantly shorter than the other helices of the bundle, and as a result, there appears to be some "wobbling" of the bottom parts of helices HB and HC with respect to the rest of the domain. This wobbling became apparent when we superimposed the "top" and "bottom" parts of the CAPPD* separately (Figure 3A,B). The superpositions resulted in much lower backbone rms deviations (0.57 ± 0.18 and 0.47 ± 0.15 Å, respectively) compared to the rms deviations derived from the superpositions of the full structures (0.95 ± 0.28 Å, Table 1).[2] The apparent gradual bend in helix HC is presumably dictated by the overall structural arrangement of the three-helix bundle, since there is no obvious local distortion of this helix as reported by the pattern of the local NOEs. Helix HC also includes an N-glycosylation site (N_{542}QS) that is present in all APP-like sequences (Figure 2). Interestingly, in PrP^{C} (the cellular isoform of prion protein), an N-glycosylation site (N_{181}IT in the human sequence) (*20*) is also localized in the middle of an α-helix.

A DALI search (http://www.ebi.ac.uk/dali) performed with the final set of CAPPD* coordinates revealed structural similarities with multiple proteins containing antiparallel α-helical bundles. These proteins are not apparently related

[2] Attempts to measure residual dipolar couplings to better define the relative orientation of the bottom region of the domain were hampered by the conditions used for structure determination.

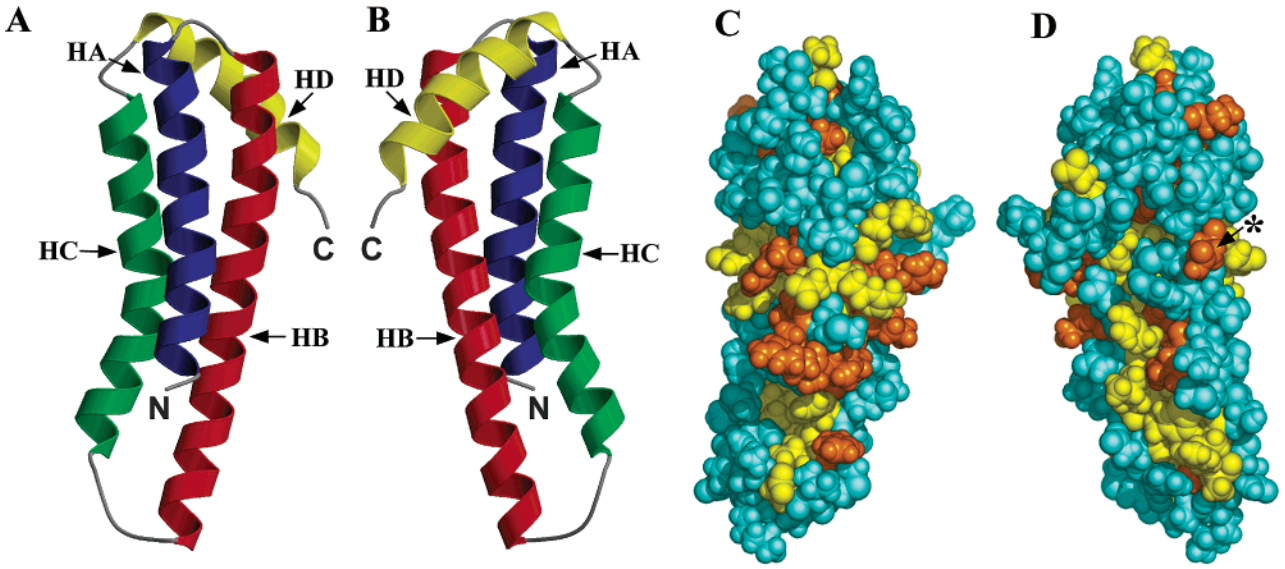

FIGURE 4: Three-dimensional structure of CAPPD*. (A and B) Ribbon diagrams of the domain in two different orientations (180° rotation along the vertical axis). The four helices are labeled: blue for HA, red for HB, green for HC, and yellow for HD. N and C denote the N- and C-terminal ends of the domain, respectively. (C and D) Space filling models of the CAPPD* in the same orientations as in panels A and B, demonstrating the high degree of evolutionary conservation of the domain. Residues shown in orange are identical in all members of the APP/APLP family, whereas residues shown in yellow are highly conserved (E/D, K/R, N/Q, I/L/V, F/W/Y, and T/S) and occur in a majority (eight of nine) of APP/APLP sequences (Figure 2). The asterisk indicates the position of the N-glycosylation site (N_{542}).

by a common biological function. The top three candidates exhibiting the lowest rmsd (from 2.6 to 3.9 Å) and a *Z*-factor of >7.5 were the N-terminal fragment of neuronal syntaxin 1a (PDB entry 1dn1), ribosome recycling factor (PDB entry 1dd5), and α-1 catenin (PDB entry 1h6g).

The sequence of CAPPD* is highly conserved through evolution and within the APP/APLP family (Figure 2; see Supporting Information Figure 1 for an alignment of the full-length proteins). Mapping the most conserved residues on the three-dimensional structure of CAPPD* shows that a large number of these residues are exposed around the surface of the domain (Figure 4C,D), suggesting that CAPPD* may be involved in physiologically important inter- and/or intramolecular interactions that are conserved in the APP/APLPs family. Such interactions could include F-spondin binding (*8*) and/or interaction of the domain with the rest of the CAPPD sequence. Indeed, the limited proteolysis data (Figure 1B) suggest that the entire CAPPD that was initially defined solely on the basis of sequence homology (*8*) may represent a structurally defined unit. Thus, in conjunction with previous studies (*5*−*7*), our results demonstrate that the extracellular sequence of APP is composed of a series of independently folded domains, consistent with the notion that APP may function as a putative cell surface receptor.

DISCUSSION

APP has been the subject of particularly intense studies because of its involvement in Alzheimer's disease (AD), one of the most common forms of progressive cognitive failure in humans. Elucidating the function of APP imposes a great scientific challenge. Despite extensive experimentation that spans techniques ranging from exhaustive biochemistry to genetic studies, the normal physiological function of APP is still elusive. Furthermore, the precise mechanism and regulation of APP cleavage, which produces amyloidogenic Aβs, are not well understood. A search for potential physiological ligands of APP that may affect APP processing constitutes a promising approach not only for understanding the biological function of APP but also for developing future therapeutics for AD. In this context, the identification of properly folded fragments corresponding to individual domains of APP and insights into their structures provide an essential basis for reliable biochemistry and, thus, will undoubtedly help us better understand this enigmatic protein. The structures of several N-terminal domains of APP have been previously reported (*5*−*7*), but there was no structural information about CAPPD.

CAPPD constitutes the largest conserved sequence of APP and is an invariant component of all APP isoforms (Figure 2). Its strategic localization next to the points of secretase action (Figure 1A) suggests that CAPPD could be centrally involved in the proteolytic processing of APP and APLPs. APLP1 and APLP2 do not yield amyloidogenic peptides upon cleavage due to substantial amino acid differences with APP in the region corresponding to Aβ sequences, but they are also physiologically processed by the same type of secretases (*21*−*23*). The notion that CAPPD may regulate cleavage of APP and APLPs has recently been supported by the finding that a putative APP ligand, F-spondin, alters APP processing by binding to CAPPD (*8*). Our current results provide the first three-dimensional structural information about this interesting region of APP.

Using limited proteolysis of a recombinant fragment of human APP, we have demonstrated that the C-terminal half of the CAPPD, which is closest to the secretase cleavage sites, constitutes an independently folded domain (Figure 1B). This domain, designated CAPPD*, forms a tightly packed, almost exclusively helical structure with a large number of highly conserved residues exposed around its entire surface (Figure 4). The high degree of conservation of the CAPPD* sequence through evolution (Figure 2) suggests that this structure is also conserved among APP/APLP family members and, thus, may perform an important biological function, although further biochemical and func-

tional studies will be required to determine whether CAPPD* is directly involved in F-spondin binding and/or APP processing. The atomic structure of CAPPD* described here provides an initial framework for understanding the function of this domain. It will also be important for uncovering the molecular mechanisms of ligand binding to this region and for the analysis of the potential effects of such interactions on APP processing. The fact that the functionally redundant APP homologues, APLP1 and APLP2, also bind F-spondin (*8*) suggests that it may be feasible to search for chemical agents that interact with the CAPPD and differentially affect APP/APLPs cleavage. This could potentially lead to a new approach for developing inhibitors of Aβ production without interfering with the essential biological function(s) of these proteins. The atomic structure of the CAPPD***** may prove to be instrumental in discovering such agents.

ACKNOWLEDGMENT

Mass spectrometry analysis of trypsin-resistant fragments was performed at the Protein Chemistry Technology Center at the University of Texas Southwestern Medical Center. N-Terminal sequencing of the fragments was performed at The Protein Chemistry Laboratory at Texas A&M University (College Station, TX).

SUPPORTING INFORMATION AVAILABLE

A full-length sequence alignment of multiple members of the APP/APLP family (Supporting Information Figure 1) and a superposition of $^{1}H-^{15}N$ HSQC spectra of CAPPD* in the presence or absence of 300 mM GdnHCl and higher NaCl concentrations (Supporting Information Figure 2). This material is available free of charge via the Internet at http://pubs.acs.org.

REFERENCES

1. De Strooper, B., and Annaert, W. (2000) Proteolytic processing and cell biological functions of the amyloid precursor protein, *J. Cell Sci. 113*, 1857−1870.
2. Selkoe, D. J. (2001) Alzheimer's disease: genes, proteins, and therapy, *Physiol. Rev. 81*, 741−766.
3. von Koch, C. S., Zheng, H., Chen, H., Trumbauer, M., Thinakaran, G., van der Ploeg, L. H., Price, D. L., and Sisodia, S. S. (1997) Generation of APLP2 KO mice and early postnatal lethality in APLP2/APP double KO mice, *Neurobiol. Aging 18*, 661−669.
4. Heber, S., Herms, J., Gajic, V., Hainfellner, J., Aguzzi, A., Rulicke, T., von Kretzschmar, H., von Koch, C., Sisodia, S., Tremml, P., Lipp, H. P., Wolfer, D. P., and Muller, U. (2000) Mice with combined gene knock-outs reveal essential and partially redundant functions of amyloid precursor protein family members, *J. Neurosci. 20*, 7951−7963.
5. Rossjohn, J., Cappai, R., Feil, S. C., Henry, A., McKinstry, W. J., Galatis, D., Hesse, L., Multhaup, G., Beyreuther, K., Masters, C. L., and Parker, M. W. (1999) Crystal structure of the N-terminal, growth factor-like domain of Alzheimer amyloid precursor protein, *Nat. Struct. Biol. 6*, 327−331.
6. Barnham, K. J., McKinstry, W. J., Multhaup, G., Galatis, D., Morton, C. J., Curtain, C. C., Williamson, N. A., White, A. R., Hinds, M. G., Norton, R. S., Beyreuthe, K., Masters, C. L., Parker, M. W., and Cappai, R. (2003) Structure of the Alzheimer's disease amyloid precursor protein copper binding domain. A regulator of neuronal copper homeostasis, *J. Biol. Chem. 278*, 17401−17407.
7. Hynes, T. R., Randal, M., Kennedy, L. A., Eigenbrot, C., and Kossiakoff, A. A. (1990) X-ray crystal structure of the protease inhibitor domain of Alzheimer's amyloid β-protein precursor, *Biochemistry 29*, 10018−10022.
8. Ho, A., and Südhof, T. C. (2004) Binding of F-spondin to amyloid-β precursor protein: a candidate amyloid-β precursor protein ligand that modulates amyloid-β precursor protein cleavage, *Proc. Natl. Acad. Sci. U.S.A. 101*, 2548−2553.
9. Guan, K. L., and Dixon, J. E. (1991) Eukaryotic proteins expressed in *Escherichia coli*: an improved thrombin cleavage and purification procedure of fusion proteins with glutathione S-transferase, *Anal. Biochem. 192*, 262−267.
10. Hakes, D. J., and Dixon, J. E. (1992) New vectors for high level expression of recombinant proteins in bacteria, *Anal. Biochem. 202*, 293−298.
11. Garcia, J., Gerber, S. H., Sugita, S., Südhof, T. C., and Rizo, J. (2004) A conformational switch in the Piccolo C2A domain regulated by alternative splicing, *Nat. Struct. Mol. Biol. 11*, 45−53.
12. Zhang, O., Kay, L. E., Olivier, J. P., and Forman-Kay, J. D. (1994) Backbone ^{1}H and ^{15}N resonance assignments of the N-terminal SH3 domain of drk in folded and unfolded states using enhanced-sensitivity pulsed field gradient NMR techniques, *J. Biomol. NMR 4*, 845−858.
13. Kay, L. E., Xu, G. Y., and Yamazaki, T. (1994) Enhanced-Sensitivity Triple-Resonance Spectroscopy with Minimal H_2O Saturation, *J. Magn. Reson., Ser. A 109*, 129−133.
14. Muhandiram, D. R., and Kay, L. E. (1994) Gradient-Enhanced Triple-Resonance 3-Dimensional NMR Experiments with Improved Sensitivity, *J. Magn. Reson., Ser. B 103*, 203−216.
15. Kay, L. E., Xu, G. Y., Singer, A. U., Muhandiram, D. R., and Formankay, J. D. (1993) A Gradient-Enhanced Hcch Tocsy Experiment for Recording Side-Chain H-1 and C-13 Correlations in H_2O Samples of Proteins, *J. Magn. Reson., Ser. B 101*, 333−337.
16. Delaglio, F., Grzesiek, S., Vuister, G. W., Zhu, G., Pfeifer, J., and Bax, A. (1995) NMRPipe: a multidimensional spectral processing system based on UNIX pipes, *J. Biomol. NMR 6*, 277−293.
17. Johnson, B. A., and Blevins, R. A. (1994) NMR View: a computer program for visualization and analysis of NMR data, *J. Biomol. NMR 4*, 603−614.
18. Cornilescu, G., Delaglio, F., and Bax, A. (1999) Protein backbone angle restraints from searching a database for chemical shift and sequence homology, *J. Biomol. NMR 13*, 289−302.
19. Brunger, A. T., Adams, P. D., Clore, G. M., DeLano, W. L., Gros, P., Grosse-Kunstleve, R. W., Jiang, J. S., Kuszewski, J., Nilges, M., Pannu, N. S., Read, R. J., Rice, L. M., Simonson, T., and Warren, G. L. (1998) Crystallography & NMR system: A new software suite for macromolecular structure determination, *Acta Crystallogr. D54*, 905−921.
20. James, T. L., Liu, H., Ulyanov, N. B., Farr-Jones, S., Zhang, H., Donne, D. G., Kaneko, K., Groth, D., Mehlhorn, I., Prusiner, S. B., and Cohen, F. E. (1997) Solution structure of a 142-residue recombinant prion protein corresponding to the infectious fragment of the scrapie isoform, *Proc. Natl. Acad. Sci. U.S.A. 94*, 10086−10091.
21. Scheinfeld, M. H., Ghersi, E., Laky, K., Fowlkes, B. J., and D'Adamio, L. (2002) Processing of β-amyloid precursor-like protein-1 and -2 by γ-secretase regulates transcription, *J. Biol. Chem. 277*, 44195−44201.
22. Walsh, D. M., Fadeeva, J. V., LaVoie, M. J., Paliga, K., Eggert, S., Kimberly, W. T., Wasco, W., and Selkoe, D. J. (2003) γ-Secretase cleavage and binding to FE65 regulate the nuclear translocation of the intracellular C-terminal domain (ICD) of the APP family of proteins, *Biochemistry 42*, 6664−6673.
23. Li, Q., and Südhof, T. C. (2004) Cleavage of amyloid-β precursor protein and amyloid-β precursor-like protein by BACE 1, *J. Biol. Chem. 279*, 10542−10550.
24. Laskowsky, R. A., MacArthur, M. W., Moss, D. S., and Thornton, J. M. (1993) PROCHECK: a program to check stereochemical quality of protein structure coordinates, *J. Appl. Crystallogr. 26*, 283−291.

BI049041O